Relating magnetic susceptibility (MS) to the simulated thematic mapper (TM) bands of the Chinese loess: Application of TM image for soil MS mapping on Loess Plateau

Junfeng Ji,[1] Jun Chen,[1] Li Jin,[1] Wanchang Zhang,[2] William Balsam,[3] and Huayu Lu[4]

Received 30 August 2003; revised 5 April 2004; accepted 15 April 2004; published 27 May 2004.

[1] Magnetic susceptibility (MS) is a very important physical attribute of the Earth's soils and surficial sediments. Soil-containing deposits in the Loess Plateau of central China offer a unique opportunity to study the relationship between soil reflectance and MS. In this paper, data on MS and diffuse reflectance spectra obtained from seven Loess Plateau sections were used to establish quantitative relationships between MS and spectral parameters related to remote sensing. By integrating the diffuse reflectance values corresponding to thematic mapper (TM) channels, five TM bands were simulated and served as independent variables for a multiple linear regression relating the bands to MS. The resulting calibration equation provides good estimates of MS values and has excellent correlation coefficients, >0.90, for all the test samples. The application of the regression equation for mapping soil MS was performed using the enhanced TM image from northwest part of Loess Plateau. The MS values obtained from TM data are convincing and compare well with the limited field test data. The spatial MS variations on the TM image clearly show a decrease toward the northwest and are in a good agreement with the monsoon directions. Results of this study demonstrate that the surface MS signal in soil can be mapped with data from satellite-based remote sensors operating in the visible and near-infrared bands. The future possibilities of this method in other soil types and climates need to be explored. *INDEX TERMS:* 5470 Planetology: Solid Surface Planets: Surface materials and properties; 0933 Exploration Geophysics: Remote sensing; 1512 Geomagnetism and Paleomagnetism: Environmental magnetism; 1694 Global Change: Instruments and techniques; 0634 Electromagnetics: Measurement and standards; *KEYWORDS:* diffuse reflectance spectroscopy, loess, magnetic susceptibility, remote sensing, thematic mapper

Citation: Ji, J., J. Chen, L. Jin, W. Zhang, W. Balsam, and H. Lu (2004), Relating magnetic susceptibility (MS) to the simulated thematic mapper (TM) bands of the Chinese loess: Application of TM image for soil MS mapping on Loess Plateau, *J. Geophys. Res.*, *109*, B05102, doi:10.1029/2003JB002769.

1. Introduction

[2] Soil-containing loess deposits and loess-derived soils are widespread, covering more than 10 percent of the land surface of the Earth. Their distribution is restricted to certain areas in arid and semiarid climates, mainly former periglacial regions approximately adjacent to glacial till areas or to deserts. Magnetic susceptibility (MS) is a very important physical parameter of loess and soil. It can be used as a proxy indicator of paleoclimate change [*Liu*, 1985; *An et al.*, 1991; *Verosub et al.*, 1993; *Heller and Evans*, 1995], hydrocarbon microseepage [*Saunders et al.*, 1999] and soil erosion, degradation, and contamination [*Petrovsky et al.*, 2000; *Ventura et al.*, 2001; *Gennadiev et al.*, 2002]. Since MS is a function of the concentration of magnetic minerals, primarily magnetite and maghemite, which exhibit diagnostic features in the visible (VIS) and near-infrared (NIR) spectra [*Sherman et al.*, 1982; *Clark et al.*, 1993; *Jin et al.*, 2003], MS should correlate to spectral reflectance in these wavelength regions [*Jin et al.*, 2003]. In addition to the minerals responsible for variations in MS, diffuse reflectance spectroscopy is also very sensitive to Fe oxides and oxyhydroxides in soils and sediments and has been used as an ancillary method to identify iron oxide minerals and estimate Fe oxide concentrations in soils and sediments [*Kosmas et al.*, 1986; *Deaton and Balsam*, 1991; *Scheinost et al.*, 1998; *Ji et al.*, 2002].

[3] On the Loess Plateau of central China, MS of the soil-containing loess deposits has been extensively studied since the early 1980s because it is a measure of the degree of pedogenic activity and serves as a proxy indicator of the

[1]Institute of Surficial Geochemistry, State Key Laboratory of Mineral Deposit Research, Department of Earth Sciences, Nanjing University, Nanjing, China.
[2]International Institute of Earth System Sciences, Nanjing University, Nanjing, China.
[3]Department of Geology, University of Texas at Arlington, Arlington, Texas, USA.
[4]State Key Laboratory of Loess and Quaternary Geology, Institute of Earth Environment, Chinese Academy of Sciences, Xian, China.

0148-0227/04/2003JB002769$09.00

summer monsoon [*Liu*, 1985; *An et al.*, 1991; *Verosub et al.*, 1993]. Magnetic enhancement is typically observed as an increase in low-field susceptibility and frequency dependence. Previous studies indicate that susceptibility enhancement is caused by the concentration of ultrafine magnetite and maghemite grains in the paleosols [*Verosub et al.*, 1993; *Heller and Evans*, 1995; *Maher*, 1998]. The alternations of loess and paleosol beds are shown by magnetic susceptibility and color reflectance variation [*Liu*, 1985; *Ji et al.*, 2001]. Regressions of susceptibility versus gray scale intensity data [*Porter et al.*, 2001] and whiteness data [*Chen et al.*, 2002] for sections in a range of climatic and latitudinal settings display a high degree of correlation. More recently, we demonstrated that near-infrared diffuse reflectance spectroscopy can successfully estimate the MS of loess-paleosol deposits on the Loess Plateau [*Jin et al.*, 2003]. These parameters therefore provide an excellent opportunity for exploring the relationship between spectral reflectance and MS for remote sensing purposes.

[4] Remote sensing data from spectrometers are commonly used in soil surveys because of documented relationships between reflectance and soil properties such as iron oxides, organic matter, clay minerals, color and moisture [*Madeira et al.*, 1997; *Palacios-Orueta and Ustin*, 1998; *Leone and Sommer*, 2000; *Galvao et al.*, 2001; *Goldshleger et al.*, 2001; *Leone and Escadafal*, 2001; *Thomasson et al.*, 2001; *Ben-Dor*, 2002]. Although magnetic susceptibility is a promising quantitative technique in many applications, it has received little attention in satellite-based remote sensing studies. The objective of this study is to examine the relationships between MS and reflectance data and to develop a regression model that can be utilized by remote sensing equipment to map MS in soils and sediments.

2. Materials and Methods

2.1. Background of Loess Deposition on Loess Plateau of Central China

[5] The loess deposits on the Loess Plateau of north central China, which cover an area of about 440,000 km^2, are transported by winds from the inland deserts in northern and northwestern China [*Liu*, 1985]. The thickness of the loess deposits in the central and southern parts of the Loess Plateau ranges from 130 to 180 m, and over 30 loess-soil (paleosol) units are recognizable within the loess deposits [*Kukla and An*, 1989; *Liu*, 1985]. Loess units are characterized by a yellowish color, a massive structure, and high carbonate contents, whereas paleosols exhibit a brownish or reddish color and pedogenic features [*Liu and Ding*, 1998]. Loess beds are interpreted as having been deposited during glacial periods when climate in north China was arid, with sparse vegetation cover and a high atmospheric dust influx. In contrast, soils developed under relatively humid conditions, with significantly reduced dust deposition on the Loess Plateau [*Liu*, 1985].

[6] On the Loess Plateau there are geographic gradients from the northwest toward the southeast, that is, from the Gobi Desert toward the wetter areas of central China. Toward the southeast rainfall increases, temperature increases, dust deposition decreases, the thickness of the loess deposits decreases, and the grain size of the loess and paleosol sediment decreases [*Liu*, 1985]. These gradients are well defined in the Malan loess layer (L1) of the last glacial age. That is, from northwest to southeast the Malan loess varies from sandy loess to silty loess and finally to clayey loess [*Liu*, 1985]. In addition to grain size, the Malan loess also displays systematic variations with respect to MS, $CaCO_3$ content, ratios of SiO_2/Al_2O_3, FeO/Fe_2O_3, dry volume density, porosity and thickness [*Liu*, 1985; *Lu and Sun*, 2000].

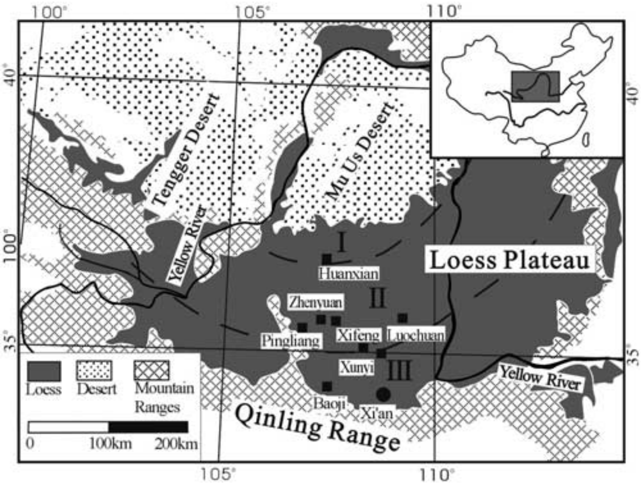

Figure 1. Sketch map of the Loess Plateau showing localities of loess-paleosol sections used in this study. Roman numerals indicate the type of loess: I, sandy loess; II, silty loess; and III, clayey loess.

2.2. Study Area and Methods

2.2.1. Study Area

[7] Samples were taken from seven loess and paleosol sections. From north to south these sections are Huanxian (36.37°N, 107.19°E), Zhengyuan (35.70°N, 107.19°E), Xifeng (35.38°N, 107.25°E), Luochuan (35.80°N, 109.40°E), Pingliang (35.54°N, 106.68°E), Xunyi (35.18°N, 108.32°E), and Baoji (34.20°N, 107.00°E) (Figure 1). The Huanxian section was sampled at a 25 cm interval, all other sections were sampled at a 20 cm interval. Our analyses of these loess sections concentrated on the early Holocene soil (S0), the Malan loess (L1), and the last interglacial paleosol (S1). Thermoluminescence (TL) dating indicates that L1 was deposited in marine oxygen isotope stages 2–3 and S1 during isotope stage 5 [*An et al.*, 1991; *Liu*, 1985]. Stratigraphy parallels changes in color and brightness; the loess is yellow and bright (high reflectivity) whereas the paleosols are red and dark (low reflectivity) [*Porter*, 2000; *Ji et al.*, 2001; *Chen et al.*, 2002].

2.2.2. Magnetic Susceptibility

[8] Paleosol layers generally exhibit high magnetic susceptibility values. Bulk magnetic susceptibility in paleosols is about 2–4 times as high as in loess beds [*Liu*, 1985; *An et al.*, 1991; *Lu and Sun*, 2000]. The magnetic susceptibility of loess and paleosol is related to the magnetic mineral species, their concentration and grain size [*Heller and Evans*, 1995; *Maher*, 1998]. The major carriers of the susceptibility are very fine particles of magnetite and maghemite, mostly smaller than 1 μm [*Heller and Evans*, 1995]. Such ultrafine magnetic minerals are now widely accepted to have a

pedogenic origin in warmer and/or wetter climates [*Verosub et al.*, 1993; *Maher*, 1998].

[9] The magnetic susceptibility of each sample was determined with a Bartington MS2 susceptibility meter, and is expressed as 10^{-8} m^3/kg [*An et al.*, 1991; *Ding et al.*, 1993; *Lu and Sun*, 2000].

2.2.3. Spectral Reflectance Measurements

[10] Reflectance spectra of samples were analyzed with a Perkin-Elmer Lambda 900 spectrophotometer with a 150 mm reflectance sphere from 190 to 2500 nm, that is, from the near ultraviolet (NUV, 190–400 nm), through the visible (VIS, 400–700 nm), and into the near infrared (NIR, 700–2500 nm).

[11] Sample preparation and analysis followed procedures described by *Balsam and Deaton* [1991] and *Ji et al.* [2002]. Samples were ground to <38 μm with a mortar and pestle, made into a thick slurry on a glass microslide with distilled water, smoothed and dried slowly at low temperature (<40°C). Data are written directly to a computer disk at 2 nm intervals as percent reflectance relative to the Spectralon standard.

2.2.4. Calculation of Simulated TM Bands

[12] The calculation of simulated TM bands follows the method proposed by *Madeira et al.* [1997]. Radiometric values recorded by satellite sensors are proportional to the luminance in the spectral band weighted by the sensor's sensitivity for the wavelength considered. A TM band can be simulated by integrating the diffuse reflectance values corresponding to this spectral window weighted by sensor's relative spectral response. This value is then the simulation of a spectral band that is called simulated TM (STM), and calculated according to

$$\mathrm{STM}_i = 255\frac{\sum_{\lambda_{1i}}^{\lambda_{2i}} R(\lambda)S_i(\lambda)}{\sum_{\lambda_{1i}}^{\lambda_{2i}} S_i(\lambda)}, \tag{1}$$

where STM_i is reflectance in the spectral band of *i*th TM channel, $R(\lambda)$ is diffuse reflectance for wavelength λ, $S_i(\lambda)$ is the sensitivity function of the TM sensor for wavelength λ in channel I, λ_{1i} and λ_{2i} are lower and upper boundaries of spectral band *i*. The constant 255 is used to scale the STM values between 0 and 255 for future image processing. (Figures for the relative spectral response for the Lansat TM7 sensor are available from www.nasa.gov.) These new variables, STM1 (0.45–0.52 μm), STM2 (0.52–0.60 μm), STM3 (0.63–0.69 μm), STM4 (0.76–0.90 μm), STM5 (1.55–1.75 μm), STM7 (2.08–2.35 μm), derived from diffuse reflectance spectra are used to model loess MS.

[13] Accurate estimates of STM_i depends upon the precise reversion of $R(\lambda)$ from the imagery under analyses. Image processing included a topographic correction, atmospheric correction and the calculation of the related radiance parameters. First, topographic correction for +ETM images using a high-resolution DEM is conducted in the accurate retrieval of the surface reflectance. The normalization algorithm proposed by *Civico* [1989] based on the relief shadow effect for Landsat TM images is used in this study. This process integrates the geometrically corrected TM/+ETM images with a DEM of the same spatial resolution to construct the shaded relief model corresponding to the solar illumination conditions at the time of the Landsat overpass. The topographically normalized images are derived through a linear transformation for each of the original TM/+ETM bands according to

$$\delta\mathrm{DN}_{\lambda_{ij}} = \mathrm{DN}_{\lambda_{ij}} + \mathrm{DN}_{\lambda_{ij}} * (\mu_k - X_{ij})/\mu_k, \tag{2}$$

where $\delta\mathrm{DN}_{\lambda_{ij}}$ stands for the normalized radiance data, $\mathrm{DN}_{\lambda_{ij}}$ stands for the raw radiance data for pixel *ij* in band λ, μ_k is the mean value for entire scaled [0, 255] illumination model, and X_{ij} is the scaled [0, 255] illumination value.

[14] Following topographic normalization of the image, an atmospheric correction algorithm [*Gilabert et al.*, 1994; *Zhang et al.*, 2001] was performed to automatically retrieve the diffuse reflectance from each band of TM/+ETM images. The model is based on three assumptions: (1) the Earth's surface is Lambertian in nature; (2) in the darkest pixels of TM bands 1 and 3, only the atmosphere contributed to radiance and the land surface reflectance is close to zero; and (3) the multiple scattering in the atmosphere and the adjacent pixel effect are negligible.

[15] Under assumption (1), surface reflectance can be calculated according to

$$R_s[\lambda] = \{K * (L_0[\lambda] - L_p[\lambda])\}/\{E_g[\lambda] * T_u(\lambda) * \cos\theta_0\}, \tag{3}$$

where λ is the central band length of different TM/+ETM bands, K is the distance between the sun and the Earth at which the scene was acquired, θ_0 is solar zenith angle, $L_0[\lambda]$ is the sensor received radiance, $L_p[\lambda]$ is the atmospheric radiance, $E_g[\lambda]$ is the total radiance of the surface, and $T_u(\lambda)$ is the upward atmospheric transmittance.

[16] Sensor received radiance, $L_0[\lambda]$, can be calculated simply as

$$L_0[\lambda] = A_1 * \mathrm{DN}[\lambda] + A_0, \tag{4}$$

where A_1 and A_0 are the calibration coefficients which vary with each band of the Landsat TM/+ETM image and are equal to the gains and offset respectively in TM/+ETM data head file.

[17] The atmospheric radiance, $L_p[\lambda]$, consists of two parts, the Rayleigh ($L_r[\lambda]$) and aerosol ($L_a[\lambda]$) contribution radiance:

$$L_p[\lambda] = L_r[\lambda] + L_a[\lambda]. \tag{5}$$

In this model, the dark pixel should be carefully selected from a shadowed cloud or mountain after the topographic correction. For the dark pixel, sensor received radiance, according to assumption (2), is approximately the atmospheric contributed to radiance:

$$L_0^*[\lambda] \approx L_p^*[\lambda], \tag{6}$$

where the asterisk refers to the selected dark pixels in TM/+ETM bands 1 and 3.

[18] As for Rayleigh radiance, the optical thickness for the ozone $\tau_{oz}(\lambda)$ can be interpolated from the values

reported by *Sturm* [1981] and the molecular optical thickness $\tau_r(\lambda, h)$ can also be obtained according to *Saunders et al.* [1999]. Aerosol contributed radiance ($L_a^*[\lambda]$), can be calculated according to formulae (4)–(6).

[19] Once $L_p[1]$ and $L_p[3]$ have been computed from the dark pixel, it is possible to calculate atmosphere radiance of other bands. Rayleigh contributed radiance, $L_r[\lambda]$, is practically constant in the atmosphere and only dependent on the solar and view zenith angles θ (in this case, θ = 0). Aerosol contributed radiance has the following relationship to band length:

$$L_a[\lambda] = \Gamma\lambda^{-\delta}, \tag{7}$$

in which Γ, δ are two basic parameters of concentration and size distribution of the aerosol particles in atmosphere and can be calculated from dark pixels in TM/+ETM band 1 and band 3 with equations (6) and (7). The other parameters, such as aerosol optical thickness $\tau_a(\lambda)$, upward and downward atmosphere transmittance, were calculated strictly following *Gilabert et al.* [1994].

[20] Finally, with the topographical effect removed, atmospheric corrected images of the scene utilized for MS mapping in this study was obtained with a accuracy about 90% [*Zhang et al.*, 2001]. The original scene utilized for this study was acquired on 14 November 2001. Pass/row of the images combined in the scene for the current study is 128/34 and 128/35, respectively.

2.2.5. Multiple Regression

[21] There are many ways to relate independent variables (STM bands or spectral values at specified wavelengths) to dependent variables (instrumentally determined component values such as magnetic susceptibility). The simplest model relates a single independent variable to the dependent variable by linear regression. For natural materials a single independent variable does not generally provide an adequate model; rather, the combined influence of several independent variables usually improves estimates of the dependent variable. A multiple regression therefore is more appropriate for relating spectral wavelengths to sediment components [*Balsam and Deaton*, 1996; *Ji et al.*, 2002]. For our calibration data set a multiple linear regression model was sufficient to explain most of the variability. As with any regression model, results are only reliable where the equation is interpolating, that is, between the minimum and maximum values of the dependent variables in the calibration database. This means our regression equation should be most accurate for MS values from 20 to 300 × 10^{-8} m^3/kg. All regressions were performed using SPSS for Windows.

[22] To investigate the relationship between MS and STM bands, a mixed data set from the Baoji and Huanxian sections was chosen as the calibration data set because these sections represent extremes, that is, end-members, in both MS values and climate. The calibration data set includes 117 samples with a wide range of MS values and therefore should provide accurate predictions of MS.

[23] Using regression techniques on the calibration data set, we established a calibration equation that related known values of MS to STM bands. This calibration equation was then applied to the test data sets to provide quantitative predictions of MS that could be compared to the instrumentally determined values from the same samples. To evaluate the success of these predictions, we used the correlation coefficient and the root-mean-square error (RMSE) given by

$$\mathrm{RMSE} = \left[\sum (y-x)^2/(n)\right]^{1/2},$$

where x is the MS value measured by the Bartington MS2, y is the predicted value from the regression calibration equation, and n is the number of samples.

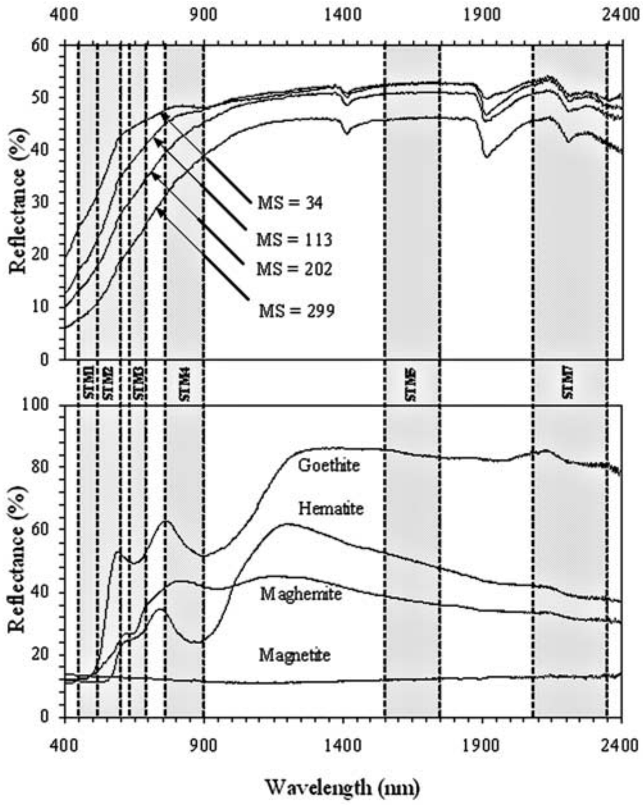

Figure 2. Reflectance spectra of the Chinese loess samples with different magnetic susceptibility values (MS unit, 10^{-8} m^3/kg) and the iron oxide minerals goethite, hematite, maghemite, and magnetite. The positions of the Landsat thematic mapper bands are shown.

3. Results and Discussion

3.1. Spectral Reflectance of the Chinese Loess

[24] Spectra of typical loess and paleosol samples, differing in their MS, are shown in Figure 2. These spectra are characterized by distinct absorption bands at 1400, 1900, and 2200 nm. The bands result from the presence of −OH either in soil minerals (at 1400 and 2200 nm) or in water molecules, adsorbed or bound (at 1900 nm). A minor but poorly defined absorption band is present at 2340 nm and is related to the presence of calcite in the samples. Additional absorption bands are centered near 900 nm due to Fe^{3+}. In the visible region there is a significant decrease in reflectance below 700 nm due to a charge transfer absorption of iron. The change of

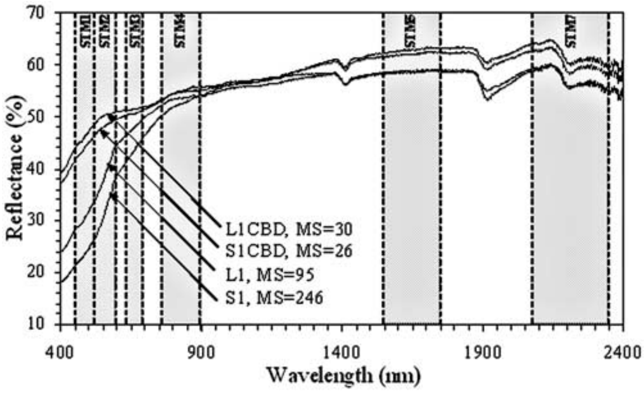

Figure 3. Comparisons of the reflectance spectra of the post-CBD treated loess (L1 CBD) and paleosol (S1 CBD) samples with their parental bulk samples (L1 and S1). This diagram illustrates that the removal of iron oxides by CBD can significantly increase the reflectance intensity of paleosol samples and reduce their magnetic susceptibility values (MS unit, 10^{-8} m^3/kg). The positions of the Landsat thematic mapper bands are shown in gray.

slope in this area is attributed to differences in iron oxide and organic matter content [*Deaton and Balsam*, 1991; *Palacios-Orueta and Ustin*, 1998].

[25] The spectral patterns of loess and paleosol samples exhibit similar trends as a function of MS; reflectance decreases in all wavelength bands as MS increases (Figure 2). Comparison of reflectance measurements to MS indicates that samples with higher average reflectance are from loess and have low susceptibilities whereas samples with lower reflectance are from paleosols and have high susceptibilities. This observation suggests that a correlation may exist between MS and spectral reflectance.

[26] To understand the correlation between spectral reflectance and magnetic susceptibility, it is necessary to know the cause of reflectance changes in loess and paleosol. Spectral reflectance intensity generally increases as the concentration of light minerals (mainly carbonate) increases, and decreases as the concentration of dark minerals (especially iron oxide, clay minerals, and organic matter) increases [*Ji et al.*, 2002; *Chen et al.*, 2002]. The recent leaching experiments [*Chen et al.*, 2002] on loess and paleosol samples demonstrated that the fine-grained iron oxide minerals are the primary factor controlling the spectral reflectance changes, whereas carbonate and organic matter, because of their low concentrations, have a minor influence on spectral reflectance changes in loess and paleosol. For a further confirmation, the fine-grained, mostly pedogenic iron oxide was removed using the citrate-bicarbonate-dithionite (CBD) extraction procedure developed by *Mehra and Jackson* [1960]. The removal of fine-grained pedogenic iron oxide from the selected analyzed samples, gives rise to significant changes in both spectral reflectance and magnetic susceptibility (Figure 3). After the CBD treatment, the spectral reflectance intensity of both the treated loess and paleosol samples increased compared to their precursors, all displaying very similar reflectance spectra. The magnetic susceptibility was also reduced greatly [*Verosub et al.*, 1993], from 246×10^{-8} m^3/kg down to 26×10^{-8} m^3/kg, and 95×10^{-8} m^3/kg to 30×10^{-8} m^3/kg for paleosol and loess, respectively. We therefore conclude that the fine-grained, CBD-extractable, iron oxide minerals are the dominant factor controlling reflectance changes and magnetic susceptibility of loess and paleosol samples.

Table 1. Statistical Results of STM Bands and Magnetic Susceptibility Regression for the 117 Samples From Baoji and Huanxian Loess Sections

Bands	Equation	R^2	RMSE
	Single Linear Regression		
STM1	MS = 369.846 − 4.979 × STM1	0.876	26.626
STM2	MS = 423.523 − 4.209 × STM2	0.888	25.350
STM3	MS = 547.533 − 4.566 × STM3	0.850	29.383
STM4	MS = 787.030 − 5.949 × STM4	0.557	50.443
STM5	MS = 504.062 − 3.000 × STM5	0.213	67.201
STM7	MS = 498.168 − 3.080 × STM7	0.271	64.679
	Stepwise Multiple Linear Regression[a]		
	MS = 189.841 + 2.088 × STM2 − 12.068 × STM3 + 11.292 × STM4 − 2.798 × STM5	0.947	17.430

[a]Calibration equation used.

3.2. STM Bands as a Function of Magnetic Susceptibility

[27] The Baoji and Huanxian sections were chosen as end-members for establishing a calibration equation because they represent extremes in both magnetic susceptibility values and climate. On the Loess Plateau (Figure 1), the Huanxian section is situated in the transitional zone of desert to loess region, where sediments are coarser, the sedimentation rate is higher and soil formation is weaker. The Baoji section, at the southern part of the Loess Plateau, is within the zone of clayey loess, where the sedimentation rate is lower and soil development is better [*Liu*, 1985; *Ding et al.*, 1993]. All the other sections used in our study are

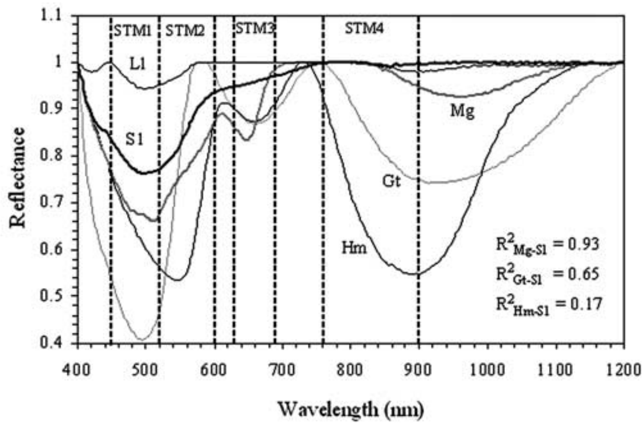

Figure 4. Continuum removed reflectance spectra of a loess sample from Huanxian section (L1, MS = 34×10^{-8} m^3/kg) and a paleosol sample from Baoji section (S1, MS = 299×10^{-8} m^3/kg), showing comparisons with maghemite (Mg), goethite(Gt) and hematite (Hm) spectra. Please note the similarity of reflectance spectra between maghemite (Mg) and paleosol (S1) samples, with a correlation coefficient (R^2) of 0.93 in the wavelength from 400 to 900 nm.

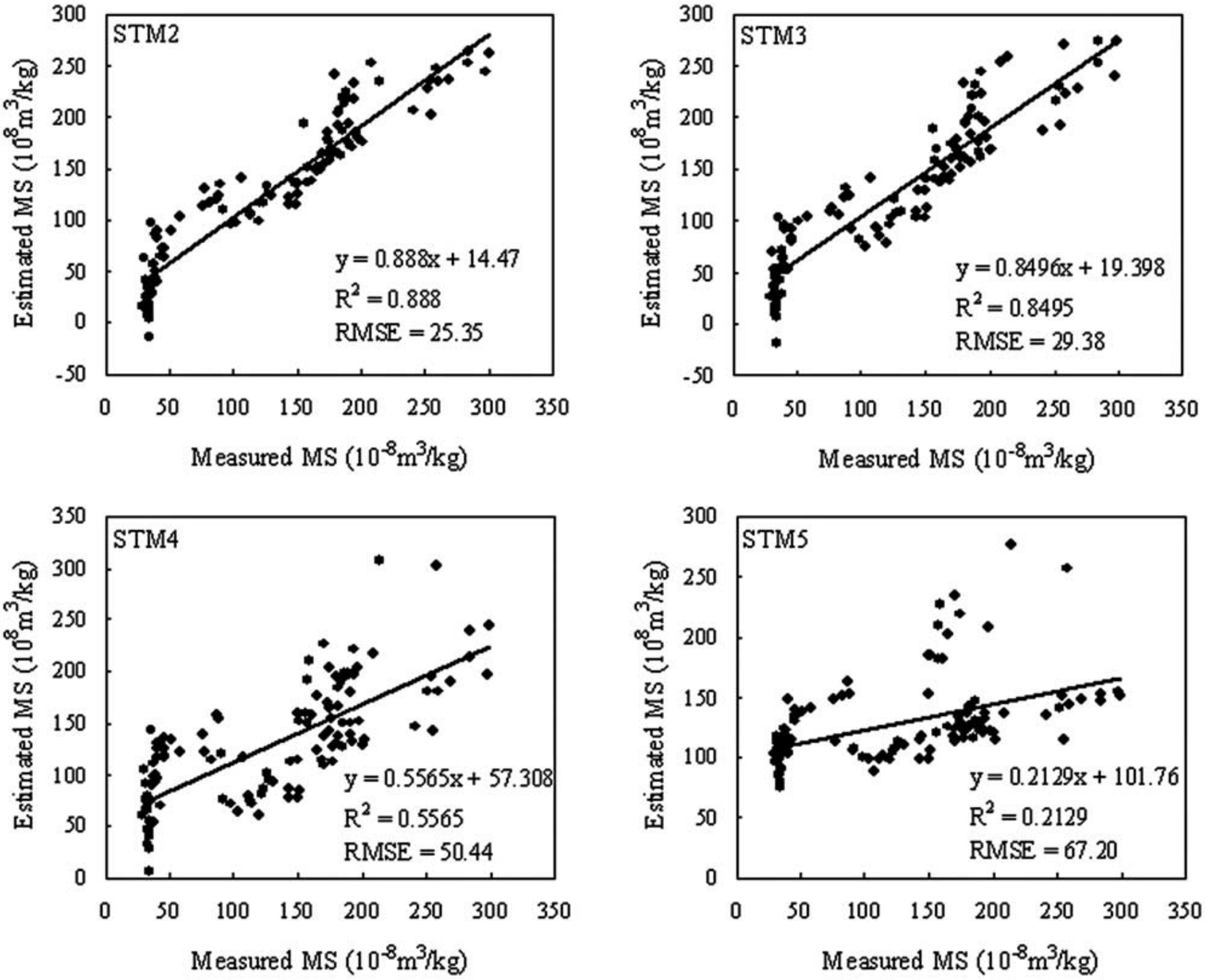

Figure 5. A comparison of instrumentally measured versus spectrally estimated magnetic susceptibility in each of bands used (STM2, 3, 4, 5) for the 117 samples from Baoji and Huanxian loess sections by using single linear regression analysis.

located in the loess zone, geographically and climatically between the Huanxian and Baoji sections and characterized by moderate soil development. The calibration data set includes 117 samples from both the Huanxian and Baoji sections with a wide range of magnetic susceptibility values (28 $\sim$ 300 SI unit) and therefore should provide accurate predictions of MS over a broad range conditions.

[28] A multiple regression equation was derived from the combination of both Baoji and Huanxian data. The multiple regression equation has 4 independent variables of STM2, STM4, STM3, and STM5 and produces a correlation coefficient of 0.973 and RMSE of ± 17 (Table 1). In the calibration equation STM2 and STM4 are positively correlated to MS, whereas STM3 and STM5 are negatively correlated to MS, and the weighting factors for the four bands used are essentially the reflectance difference between STM4 and STM3 (STM4 minus STM3). Several observations suggest this correlation results from the shape of the hematite, goethite and maghemite reflectance curves, especially maghemite (Figure 2). First, the included STM bands (STM2, STM4, STM3, and STM5) compare well with the spectral features of these iron oxide minerals, whereas the spectral region of the excluded bands, STM1 and STM7, are smooth in the spectral curve. Second, the reflectance in the bands of STM2 and STM4 that are positively correlated shows peaks or increases in the maghemite curve. The STM2 band also contains peaks for hematite and goethite, whereas the STM4 band exhibits valleys for these minerals. The STM3 and STM5 bands that are negatively correlated in the equation exhibit reflectance decreases in the wavelength range they occupy (Figure 2).

[29] To better explore the intrinsic relationship between STM bands and iron oxide minerals, a continuum removal analysis [*Clark and Roush*, 1984] is used to isolate major absorption features in the reflectance spectrum from 400 nm to 1200 nm with ENVI Version 3.5 (Figure 4). The result clearly shows a striking similarity in reflectance shape between paleosol and maghemite samples relative to hematite and goethite. The correlation coefficient (r^2)

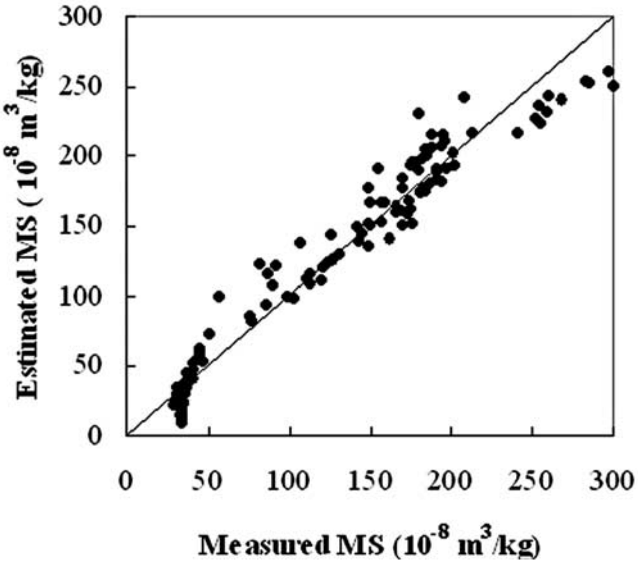

Figure 6. Instrumentally measured and spectrally estimated magnetic susceptibility for the 117 samples from Baoji and Huanxian loess sections. The line bisecting the diagram indicates where all points would lie in a perfect correlation.

between paleosol and maghemite is 0.93, much higher than that with goethite (0.65) and hematite (0.17). The maghemite displays an exactly parallel change with paleosol's in STM2 band, and a clear absorption feature in STM3 band but minor one in STM4 band, whereas hematite and goethite exhibit strong absorption features both in STM3 and STM4 bands. Bands STM2 and STM3, those bands which are highly correlated to maghemite, also exhibit a stronger correlation to MS than STM4 and STM5 (Table 1 and Figure 5).

[30] Figure 4 also clearly exhibits the difference between bands of STM3 and STM4 and their response to changes in maghemite concentration. As noted above, maghemite shows a clear absorption feature centered in the STM3 band and is mostly featureless in the long range of STM4 band. The difference in reflectance between STM4 and STM3 bands (STM4 − STM3) is indeed related to the maghemite absorption signal strength. Although MS in the Chinese loess was thought to be controlled primarily by magnetite and/or maghemite concentration (magnetite does not exhibit diagnostic reflectance features in the wavelength range we analyzed), more recent investigations may support that the magnetic mineral responsible for the enhancement of MS in paleosol is mainly the nanoscale [*Chen et al.*, 2003]/pseudo-single-domain [*Liu et al.*, 2003] maghemite [*Verosub et al.*, 1993]. Therefore our multiple regression equation is responding, at least in part, to changes in maghemite concentration, although the overall reflectance of loess soil is influenced by many other variables.

[31] The plot of instrumentally determined versus estimated MS values (Figure 6) indicates that the regression equation does a credible job estimating MS in the mixed database. However, the equation slightly underestimates both very high and very low values and slightly overestimates the values between the extremes.

[32] The model was tested by using it to estimate MS in the other five loess-paleosol profiles, the test data sets. The instrumentally determined and spectrally estimated MS exhibit similar trends (Figure 7). With the exception of the Luochuan section, all the test data sets exhibit the same trend shown in the correlation data set, that is, samples exhibiting high or low MS values are underestimated whereas those exhibiting intermediate values are only slightly overestimated. The Luochuan section exhibits more scatter, perhaps because it is farther east than the other sections (Figure 1) and experiences slightly different environmental conditions. The correlation coefficients of the five sections are all higher than 0.90, with RMSE's ranging from ±14 to ±32 and averaging ±19, demonstrating that the equation is doing a reasonable job estimating MS.

3.3. Application to Surface Samples

[33] One potential obstacle to the application of our regression equation to mapping the land surface by satellite based spectroradiometers is that our samples were collected from a vertical profile and not from soils on the land surface. To determine if subaerial conditions affected the efficacy of our equation, we collected 23 surface soil samples across the Loess Plateau from the boundary of desert and sandy loess zones to the boundary of loess and clayey loess zones in late October 2001. MS values of the surface samples range from 32 to 135 10^{-8} m^3/kg, lower than the section samples studied above, and show a north to south gradient on the Loess Plateau with the MS signal increasing to the south. We applied our calibration function to the surface samples, the results are shown in Figure 8. It reveals that there is a good correlation (r^2 = 0.9182, RMSE = ±11) between the estimated and measured MS data on these modern soil samples.

[34] The other potential obstacle to the application of our regression equation for mapping loess by remote sensing is that the samples used in our regression analysis are highly prepared soil samples, not the actual soil surfaces. To validate the ability of our regression equation to estimate the MS values of actual soil samples, reflectance spectra of the raw, unprepared samples noted above (Figure 8) were analyzed, and our calibration function was applied to these reflectance data. Our results (Figure 9) clearly indicate that there is also a good correlation (r^2 = 0.8566, RMSE = ±12) between the estimated and measured MS data on these real soil samples, but samples exhibiting high MS values (over 130 × 10^{-8} m^3/kg) are slightly underestimated with these limited data. Therefore our regression equation is capable of precisely estimating MS in modern soils suggesting that similar conditions are responsible for the relationship of MS and spectral bands today as in the past.

3.4. MS Mapping on Loess Plateau by Using TM Image

[35] In order to validate the feasibility of our function for mapping soil MS on Loess Plateau by remote sensing, it was applied to +ETM scene (see previous sections) from northwest part of Loess Plateau. The region utilized for MS mapping in this study was acquired on 14 November 2001 and covers the desert and sandy loess boundary, about 180 ×

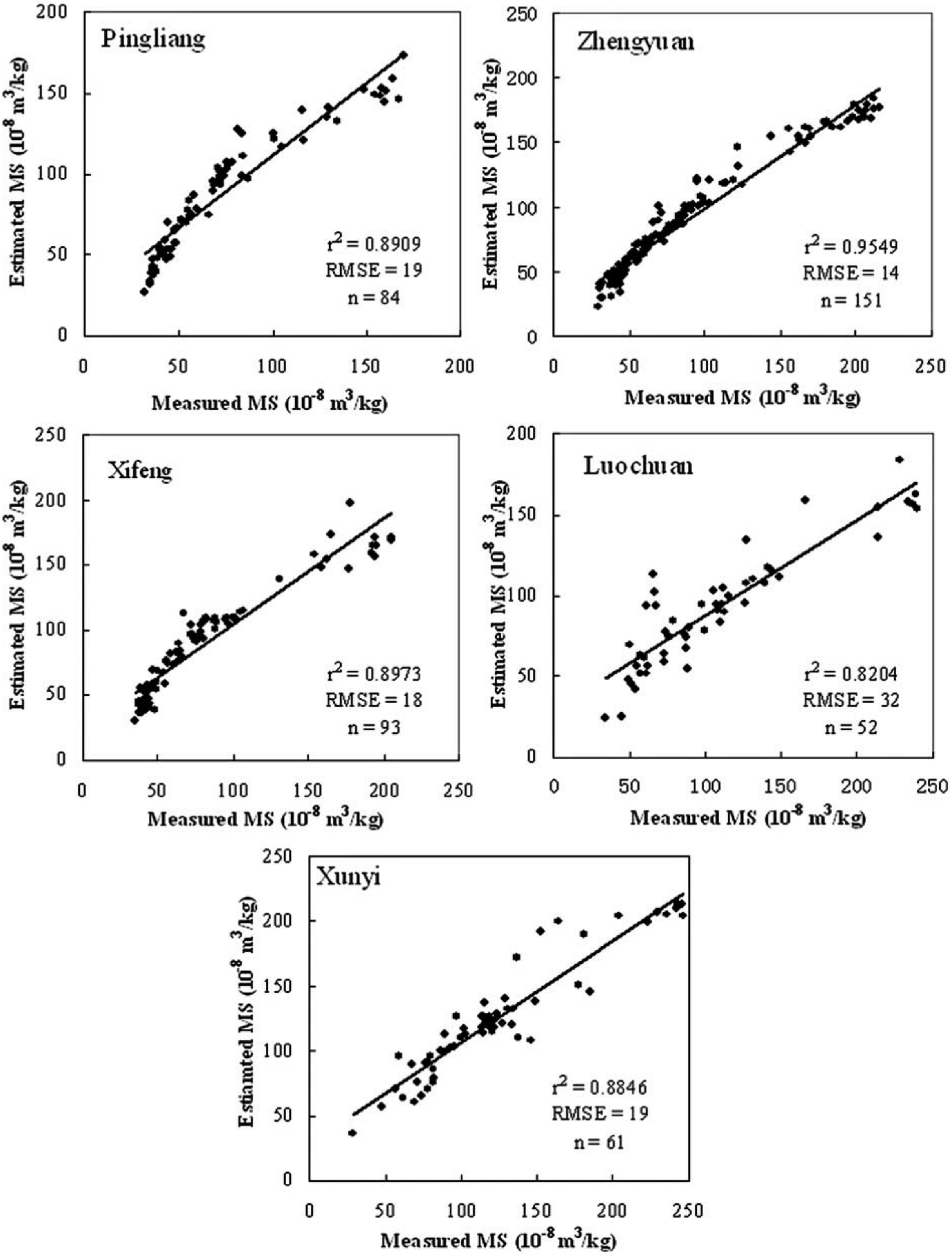

Figure 7. Data plot of instrumentally measured versus spectrally estimated magnetic susceptibility of end-member model for Pingliang, Zhengyuan, Xifeng, Luochuan, and Xunyi loess sections.

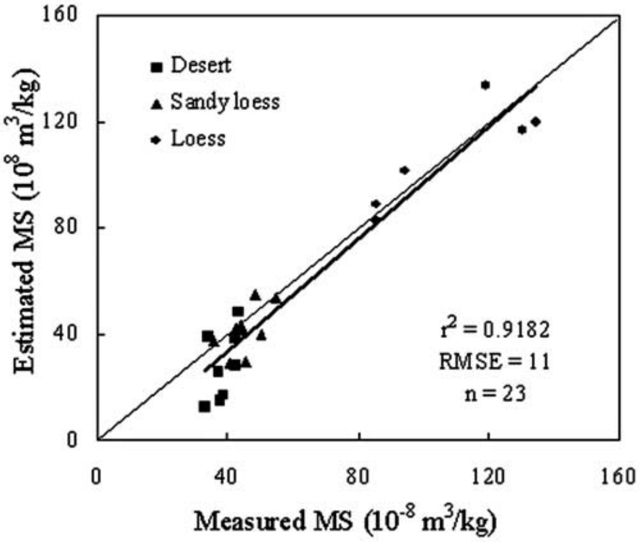

Figure 8. Instrumentally measured and spectrally estimated magnetic susceptibility for the 23 laboratory prepared surface samples from Loess Plateau.

180 km (Figure 10). This image originally consisted of two half images (the lower half part of pass128/row34 and the upper part of pass128/row35 images) which we united. It was selected for three main reasons. First, it is an arid region and vegetation cover of either trees or grass is very sparse; it is classified as desert and sandy loess. In fact, the Normalized Difference Vegetation Index (NDVI) of this TM image analyzed, calculated from the visible and near infrared TM channels as (TM 4 − TM 3)/(TM 4 + TM 3), is less than 0.12 and very low, showing very little photosynthetically active vegetation. Second, November is the start of winter season and there are wide expanses of bare soil, ready for sowing wheat, and plant remains from the previous crops and wild vegetation has been buried by plowing. Third, atmospheric effects are weak and the sky is generally clear. Image processing included a topographic correction, atmospheric correction and the calculation of the related radiance parameters as described in previous sections.

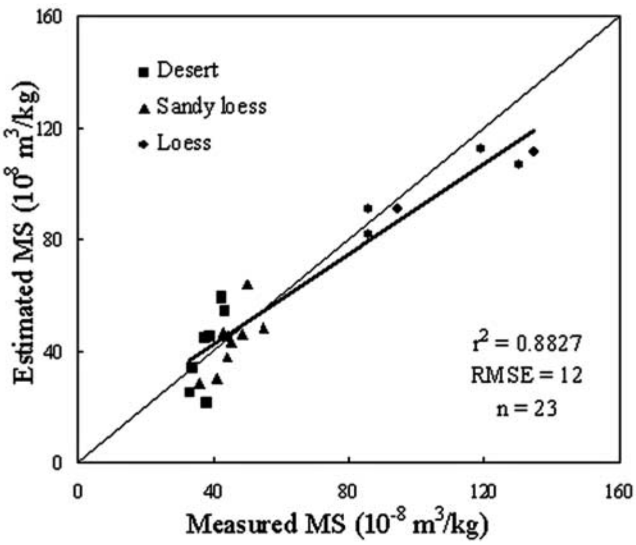

Figure 9. Instrumentally measured and spectrally estimated magnetic susceptibility for the 23 raw surface samples from Loess Plateau.

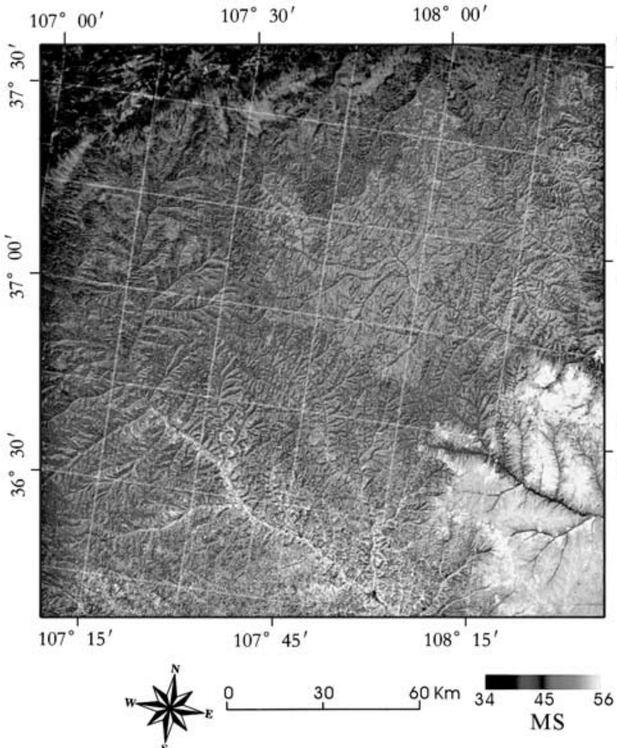

Figure 10. Mapping of magnetic susceptibility of surface soils on northwestern Loess Plateau using enhanced TM image on 14 November 2001. See color version of this figure at back of this issue.

[36] The MS mapping of surface soils on northwestern Loess Plateau using enhanced TM image on 14 November 2001 is shown in Figure 10. The MS values obtained from TM data (Figure 10) are convincing and compare well with surface sample data from the desert and sandy loess zones (Figure 8) and other available surface MS data [*Porter et al.*, 2001]. The spatial distribution of MS variations on the TM image clearly displays a southeastward increase, and is in good agreement the monsoon directions [*Liu*, 1985; *An et al.*, 1991; *Porter et al.*, 2001]. For example, the lowest MS values, about 34×10^{-8} m^3/kg, were obtained near the margin of the Mu Us desert. MS values increase southward and eastward, reaching 56×10^{-8} m^3/kg at the southeastern margin of this TM image. Therefore the regression equation based on end-member sections at Baoji and Huanxian is capable of accurately mapping MS in surface soils on Loess Plateau.

[37] The above results demonstrate the possibility of mapping variations of the soil MS signal with Landsat TM data. The use of rapidly estimated MS measurements from satellites represents a new method for mapping and measuring soil quality. The resulting MS map could be useful for identifying areas strongly affected by soil erosion, contamination, degradation, and desertification.

[38] MS measurement on topsoil and sediments has often been used as a sensitive, accurate, and useful tool during the

last few years to detect anthropogenic pollution, soil erosion pattern and hydrocarbon microseepage [*Saunders et al.*, 1999; *Petrovsky et al.*, 2000; *Ventura et al.*, 2001; *Gennadiev et al.*, 2002]. Spatial information on soil and sediment quality may be required at different scales and covering large areas resulting in a time-consuming and very expensive characterization based on soil and sediment sampling and analysis. The methodology proposed here can be used to map magnetic susceptibility and contaminated soils on a much larger scale.

[39] Remotely sensed spectral signals present some additional challenges including the nature of the loess surface, such as roughness, moisture, vegetation cover, etc., and the influence of the atmosphere and illumination [*Leone and Sommer*, 2000]. Further research on the suitability of this method for different soil types is required. Its adaptation to sensors other than thematic mapper, such as SPOT, would also be useful.

4. Conclusions

[40] Diffuse reflectance spectra obtained in the laboratory from seven loess sections on the Loess Plateau of north central China were used to establish quantitative relationships between STM bands and MS with a multiple linear regression technique. A close relationship between MS and STM bands was observed in the Chinese loess, but changes geographically from section to section. The resulting calibration equation based on end-member loess sections, provides good estimates of MS values and has an excellent correlation coefficient, >0.90, for all the test samples. In this paper we demonstrate that Loess Plateau soil MS can be mapped using spectra derived from TM sensors suggesting that the MS signal in surface horizons can be characterized directly and mapped from satellite-based space platforms. This study opens a new approach for the evaluation of soil erosion, contamination, and oil applications.

[41] **Acknowledgments.** This study was funded by the National Natural Science Foundation of China through grants 40331001 and 40273002, and by NKBRSF Project (G 1999043400). We would like to thank the Associate Editor, Stephen Park, the Editor, Francis Albarede, two anonymous reviewers, and Peng Gong for their helpful comments and suggestions for improvement of the manuscript.

References

An, Z. S., G. Kukla, S. C. Porter, and J. L. Xiao (1991), Magnetic susceptibility evidence of monsoon variation on the Loess Plateau of central China during the last 130,000 years, *Quat. Res.*, *36*, 29–36.

Balsam, W. L., and B. C. Deaton (1991), Sediment dispersal in the Atlantic Ocean: Evaluation by visible light spectra, *Rev. Aquat. Sci.*, *4*, 411–447.

Balsam, W. L., and B. C. Deaton (1996), Determining the composition of late Quaternary marine sediments from NUV, VIS, and NIR diffuse reflectance spectra, *Mar. Geol.*, *134*, 31–55.

Ben-Dor, E. (2002), Quantitative remote sensing of soil properties, *Adv. Agron.*, *75*, 173–243.

Chen, J., J. F. Ji, W. Balsam, Y. Chen, L. W. Liu, and Z. S. An (2002), Characterization of the Chinese loess-paleosol stratigraphy by whiteness measurement, *Palaeogeogr. Palaeoclimatol. Palaeoecol.*, *183*, 287–297.

Chen, T. H., H. F. Xu, J. F. Ji, J. Chen, and Y. Chen (2003), Formation mechanism of ferromagnetic minerals in loess of China: TEM investigation, *Chinese Sci. Bull.*, *48*(20), 2259–2266.

Civico, D. L. (1989), Topographic normalization of Landsat thematic mapper digital imagery, *Photogram. Eng. Remote Sens.*, *55*(9), 1303–1309.

Clark, R. N., and T. L. Roush (1984), Reflectance spectroscopy: Quantitative analysis techniques for remote sensing applications, *J. Geophys. Res.*, *89*, 6329–6340.

Clark, R. N., G. A. Swayze1, A. J. Gallagher, T. V. V. King, and W. M. Calvin (1993), The Geological Survey, U.S., Digital Spectral Library: Version 1:0.2 to 3.0 μm, *U.S. Geol. Surv. Open File Rep., 93-592*, 1340 pp.

Deaton, B. C., and W. L. Balsam (1991), Visible spectroscopy: A rapid method for determining hematite and goethite concentration in geological materials, *J. Sediment. Petrol.*, *61*, 628–632.

Ding, Z. L., N. Rutter, and T. S. Liu (1993), Pedostratigraphy of Chinese loess deposits and climatic cycles in the last 2.5 Myr, *Catena*, *20*, 73–91.

Galvao, L. S., M. A. Pizarro, and J. C. N. Epiphanio (2001), Variations in reflectance of tropical soils: Spectral-chemical composition relationships from AVIRIS data, *Remote Sens. Environ.*, *75*, 245–255.

Gennadiev, A. N., K. R. Olson, S. S. Chernyanskii, and R. L. Jones (2002), Quantitative assessment of soil erosion and accumulation processes with the help of a technogenic magnetic tracer, *Eur. Soil Sci.*, *35*, 17–29.

Gilabert, M. A., C. Conese, and F. Maselli (1994), An atmospheric correction method for the automatic retrieval of surface reflectance from TM images, *Int. J. Remote Sens.*, *15*(10), 2065–2086.

Goldshleger, N., E. Ben-Dor, Y. Benyamini, M. Agassi, and D. G. Blumberg (2001), Characterization of soil's structural crust by spectral reflectance in the SWIR region (1.2–2.5 μm), *Terra Nova*, *13*, 12–17.

Heller, F., and M. Evans (1995), Loess magnetism, *Rev. Geophys.*, *33*, 211–240.

Ji, J. F., W. Balsam, and J. Chen (2001), Mineralogic and climatic interpretations of the Luochuan loess section (China) based on diffuse reflectance spectrophotometry, *Quat. Res.*, *56*, 23–30.

Ji, J. F., W. Balsam, J. Chen, and L. W. Liu (2002), Rapid and quantitative measurement of hematite and goethite in the Chinese loess-paleosol sequence by diffuse reflectance spectroscopy, *Clays Clay Miner.*, *50*, 210–218.

Jin, L., J. Ji, W. Balsam, Y. Chen, J. Chen, and H. Lu (2003), Determining magnetic susceptibility in loess-paleosol sections by near-infrared reflectance spectroscopy, *Geophys. Res. Lett.*, *30*(10), 1520, doi:10.1029/2003GL017389.

Kosmas, C. S., D. P. Franzmeier, and D. G. Schulze (1986), Relationship among derivative spectroscopy, color, crystallite dimensions, and Al substitution of synthetic goethites and hematites, *Clays Clay Miner.*, *34*, 625–634.

Kukla, G., and Z. S. An (1989), Loess stratigraphy in central China, *Palaeogeogr. Palaeoclimatol. Palaeoecol.*, *72*, 203–225.

Leone, A. P., and R. Escadafal (2001), Statistical analysis of soil colour and spectroradiometric data for hyperspectral remote sensing of soil properties (example in a southern Italy Mediterranean ecosystem), *Int. J. Remote Sens.*, *22*, 2311–2328.

Leone, A. P., and S. Sommer (2000), Multivariate analysis of laboratory spectra for the assessment of soil development and soil degradation in the southern Apennines (Italy), *Remote Sens. Environ.*, *72*, 346–359.

Liu, Q., S. K. Banerjee, M. J. Jackson, F. Chen, Y. Pan, and R. Zhu (2003), An integrated study of the grain-size-dependent magnetic mineralogy of the Chinese loess/paleosol and its environmental significance, *J. Geophys. Res.*, *108*(B9), 2437, doi:10.1029/2002JB002264.

Liu, T. S. (1985), *Loess and the Environment*, China Ocean Press, Beijing.

Liu, T. S., and Z. L. Ding (1998), Chinese loess and the paleomonsoon, *Annu. Rev. Earth Planet. Sci.*, *26*, 111–145.

Lu, H. Y., and D. H. Sun (2000), Pathways of dust input to the Chinese Loess Plateau during the last glacial and interglacial periods, *Catena*, *40*, 251–261.

Madeira, J., A. Bedidi, B. Cervelle, M. Pouget, and N. Flay (1997), Visible spectrometric indices of hematite (Hm) and goethite (Gt) content in lateritic soils: The application of a thematic mapper (TM) image for soil-mapping in Brasilia, Brazil, *Int. J. Remote Sens.*, *18*, 2835–2852.

Maher, B. A. (1998), Magnetic properties of modern soils and Quaternary loessic paleosols: Paleoclimatic implications, *Palaeogeogr. Palaeoclimatol. Palaeoecol.*, *137*, 25–54.

Mehra, O. P., and M. L. Jackson (1960), Iron oxide removal from soils and clays by a dithionite-citrate system buffered with sodium bicarbonate, *Clays Clay Miner.*, *7*, 317–327.

Palacios-Orueta, A., and S. L. Ustin (1998), Remote sensing of soil properties in the Santa Monica Mountains I. Spectral analysis, *Remote Sens. Environ.*, *65*, 170–183.

Petrovsky, E., A. Kapicka, N. Jordanova, M. Knab, and V. Hoffmann (2000), Low-field magnetic susceptibility: A proxy method of estimating increased pollution of different environmental systems, *Environ. Geol.*, *39*, 312–318.

Porter, S. (2000), High-resolution paleoclimatic information from the Chinese eolian sediments based on grayscale intensity profiles, *Quat. Res.*, *53*, 70–77.

Porter, S. C., B. Hallet, X. Wu, and Z. An (2001), Dependence of near-surface magnetic susceptibility on dust accumulation rate and precipitation on the Chinese Loess Plateau, *Quat. Res.*, *55*, 271–283.

Saunders, D. F., K. R. Burson, and C. K. Thompson (1999), Model for hydrocarbon microseepage and related near-surface alterations, *AAPG Bull.*, *83*, 170–185.
Scheinost, A. C., A. Chavernas, V. Barron, and J. Torrent (1998), Use and limitation of second-derivative diffuse reflectance spectroscopy in the visible to near-infrared range to identify and quantify Fe oxide minerals in soils, *Clays Clay Miner.*, *46*, 528–536.
Sherman, D. M., R. G. Burns, and V. M. Burns (1982), Spectral characteristics of the iron oxides with application to the Martian bright region mineralogy, *J. Geophys. Res.*, *87*, 10,169–10,180.
Sturm, B. (1981), The atmospheric correction of remote sensing data and the quantitative determination of suspended matter in marine water surface layers, in *Remote Sensing in Meteorology, Oceanography and Hydrology*, edited by A. P. Cracknell, pp. 215–228, Ellis Horwood, Chichester, UK.
Thomasson, J. A., R. Sui, M. S. Cox, and A. Al-Rajehy (2001), Soil reflectance sensing for determining soil properties in precision agriculture, *Trans. ASAE*, *44*, 1445–1453.
Ventura, E., Jr., M. A. Nearing, and L. D. Norton (2001), Developing a magnetic tracer to study soil erosion, *Catena*, *43*, 277–291.
Verosub, K. L., P. Fine, M. J. Singer, and J. TenPas (1993), Pedogenesis and paleoclimate: Interpretation of the magnetic susceptibility record of Chinese loess-paleosol sequences, *Geology*, *21*, 1011–1014.
Zhang, W. C., Y. Yamaguchi, and K. Ogaw (2001), Evaluation of the preprocessing of the remotely sensed data on the actual evapotraspiration, surface soil moisture mapping by an approach using Landsat, DEM and meteorological data, *Geocarto Int.*, *15*(4), 57–67.

W. Balsam, Department of Geology, University of Texas at Arlington, Arlington, TX 76019, USA.

J. Chen, J. Ji, and L. Jin, Institute of Surficial Geochemistry, State Key Laboratory of Mineral Deposit Research, Department of Earth Sciences, Nanjing University, Nanjing 210093, China. (jijunfeng@nju.edu.cn)

H. Lu, State Key Laboratory of Loess and Quaternary Geology, Institute of Earth Environment, Chinese Academy of Sciences, Xian 710075, China.

W. Zhang, International Institute of Earth System Sciences, Nanjing University, Nanjing 210093, China.

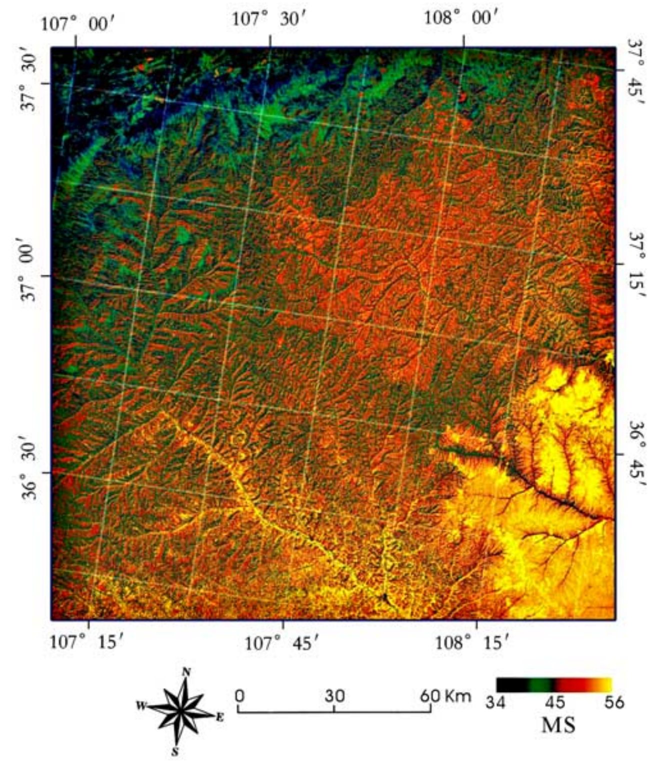

Figure 10. Mapping of magnetic susceptibility of surface soils on northwestern Loess Plateau using enhanced TM image on 14 November 2001.